Inorganica Chimica Acta 362 (2009) 3493–3501

Contents lists available at ScienceDirect

Inorganica Chimica Acta

journal homepage: www.elsevier.com/locate/ica

Mixed-ligand tris chelated complexes of Mo(IV) and W(IV): A comparative study

Amit Majumdar, Sabyasachi Sarkar *

Department of Chemistry, Indian Institute of Technology Kanpur, Kanpur 208 016, UP, India

ARTICLE INFO

Article history:
Received 1 December 2008
Received in revised form 16 March 2009
Accepted 24 March 2009
Available online 1 April 2009

Keywords:
Mixed-ligand tris chelate
Mo^{IV}
W^{IV}
Tris
N,N-diethyldithiocarbamate
2-Aminothiophenolate

ABSTRACT

Two hitherto unknown mixed-ligand tris chelated complexes containing 2-aminothiophenolate, $[Et_4N]_2[M^{IV}(NH{-}(C_6H_4){-}S)(mnt)_2]$ (M = Mo, **1a**; W, **2a**) and two mixed-ligand tris chelate complex containing N,N-diethyldithiocarbamate, $[Et_4N]_2[M^{IV}(Et_2NS_2)(mnt)_2]$ (M = Mo, **1b**; W, **2b**) have been synthesized and characterized structurally. Although these complexes are supposed to be quite similar to the well-known symmetric tris chelate complexes of maleonitriledithiolate (mnt), $[Et_4N]_2[M^{IV}(mnt)_3]$ (M = Mo, **1c**; W, **2c**), but display both trigonal prismatic and distorted trigonal prismatic geometry in their crystal structure indicating the possibility of an equilibrium between these two structural possibilities in solution. Unlike extreme stability of **1b**, **2b**, **1c** and **2c**, both **1a** and **2a** are highly unstable in solution. In contrast to one reversible reduction in case of **1b** and **2b**, **1a** and **2a** exhibited no possible reduction up to −1.2 V and two sequential oxidation steps which have been further investigated with EPR study. Differences in stability and electrochemical behavior of **1a**, **1b**, **2a** and **2b** have been correlated with theoretical calculations at DFT level in comparison with long known **1c** and **2c**.

1. Introduction

Six coordinate tris chelated complexes have attracted much attention due to their interesting structural properties. These complexes are known to adopt a trigonal prismatic structure instead of the usual octahedral geometry [1–3]. The relation between electronic state of the central metal atom and the structure of the tris chelated complex has been well established [4–7]. Electronic control of the "Bailer Twist" in formally d^0–d^2 molybdenum tris (dithiolene) complexes has recently been elegantly described [8].

M(IV) (M = Mo/W) tris(dithiolene) complexes are frequently been found as an unwanted by-product during the synthesis of model active sites of mononuclear molybdenum and tungsten enzymes [9], as these are thermodynamically most stable complexes in molybdenum(IV) and tungsten(IV) dithiolene chemistry. The redox series like $[Mo(S_2C_2Me_2]^{0,1-,2-}$ is described earlier in connection with metal dithiolene series [10]. Tris chelated Mo(V)/W(V) complexes are studied with a special emphasis to their interesting EPR spectroscopic properties [11–16] in relevance to mononuclear Mo/W enzymes.

In our endeavor in the field of structural–functional modeling for the oxidoreductase class of molybdenum and tungsten enzymes [17–20,22,23] we observed that the {M═O} moiety in the complex $[M^{IV}O(mnt)_2]^{2-}$ (M = Mo/W) can be opened up [20–23] with the addition of an acid (HX, where X is a non-coordinating or weekly coordinating anion) and utilizing different monodentate ligands the intermediate species $\{M^{IV}(OH)(X)\}$ can be converted to a diverse class of complexes exhibiting interesting model enzymatic reactions [22,23]. Use of bidentate ligand at this stage lead to the isolation of mixed-ligand tris chelated complexes **1a**, **2a**, **1b** and **2b** (Chart 1). Complex **1b** has been reported earlier as a tetrabutylammonium salt, mixed with $[Bu_4N]_2[Mo(mnt)_3]$ resulting from a tedious synthetic procedure [24] although its tungsten analogue **2b** has not been structurally characterized by X-ray. Complexes **1a** and **2a** are found to be unstable both in the solid and in solution, compared with the stable symmetric tris chelated complexes [25–34] of maleonitrile dithiolate (mnt) [35–38], **1c** and **2c** (Chart 1). On the other hand, **1b** and **2b** were found to be stable both in the solid as well as in solution state. The differing stability patterns of these mixed-ligand tris chelated complexes along with their interesting electrochemical properties are correlated with theoretical calculation at DFT level. The reversible oxidations exhibited by **1a** and **2a** have been exploited further to investigate EPR spectroscopic signatures of their one electron oxidized species.

2. Experimental

2.1. Materials and physical methods

All reactions and manipulations were performed under a pure argon atmosphere using modified Schlenk technique. 2-Aminothiophenol and CH_3SO_3H was obtained from S.D. Fine Chemicals Ltd., India. Solvents were distilled and dried by standard procedure before used. $[Ph_4P]_2[Mo^{IV}O(mnt)_2]$ and $[PNP]_2[Mo^{IV}O(mnt)_2]$ were prepared following the similar procedure for the preparation of

---

* Corresponding author. Tel./fax: +91 512 2597265.
E-mail address: abya@iitk.ac.in (S. Sarkar).

0020-1693/$ - see front matter © 2009 Elsevier B.V. All rights reserved.
doi:10.1016/j.ica.2009.03.036

Complexes	Designations
$[Et_4N]_2[Mo^{IV}(NH\text{-}(C_6H_4)\text{-}S)(mnt)_2]$	**1a**
$[Et_4N]_2[W^{IV}(NH\text{-}(C_6H_4)\text{-}S)(mnt)_2]$	**2a**
$[Et_4N]_2[Mo^{IV}((Et_2NS_2)(mnt)_2]$	**1b**
$[Et_4N]_2[W^{IV}((Et_2NS_2)(mnt)_2]$	**2b**
$[Et_4N]_2[Mo^{IV}(mnt)_3]$	**1c** [5, 24)]
$[Et_4N]_2[W^{IV}(mnt)_3]$	**2c** [5]
mnt	Maleonitriledithiolate [34-37]

Chart 1. Designations and abbreviations.

$[Et_4N]_2[Mo^{IV}O(mnt)_2]$ [17,39] by using $[Ph_4P][Br]$ and [PNP][Cl] instead of $[Et_4N][Br]$. X-ray data were collected on a Bruker-AXS Smart APEX CCD diffractometer. Infrared spectra were recorded on a Bruker Vertex 70, FT-IR Spectrophotometer as pressed KBr disks. Elemental analyses for carbon, hydrogen, nitrogen and sulfur were carried out with Perkin–Elmer 2400 microanalyser. Electronic spectra were recorded using a USB 2000 (Ocean Optics Inc.) UV–Vis spectrophotometer equipped with fiber optics. Cyclic voltammetric measurements were made with BASi Epsilon-EC Bioanalytical Systems Inc. Cyclic voltammograms of 10^{-3} M solution of the compounds (**1a**, **2a**, **1b** and **2b**) were recorded (scan rate = 100 mV/s) using glassy carbon electrode as working electrode, 0.2 M $[Bu_4N][ClO_4]$ as supporting electrolyte, Ag/AgCl electrode as reference electrode and platinum wire as an auxiliary electrode. Sample solutions were prepared in acetonitrile. Differential pulse polarography was performed with scan rate = 20 mV/s, pulse width = 50 ms, pulse period = 200 ms, pulse amplitude = 50 mV. All electrochemical experiments were done under argon atmosphere at 298 K. Potentials are referenced against internal ferrocene (Fc) and are reported relative to the Ag/AgCl electrode ($E_{1/2}(Fc^+/Fc) = 0.459$ V versus Ag/AgCl electrode).

2.2. Synthesis

*$[Et_4N]_2[Mo^{IV}(NH–(C_6H_4)–S)(mnt)_2]$ (**1a**):* To a solution of 2.62 g (4 mmol) of $[Et_4N]_2[Mo^{IV}O(mnt)_2]$ and 2.14 ml (20 mmol) of 2-aminothiophenol in 30 ml dichloromethane in cold was added 1 ml methanesulfonic acid dropwise with constant stirring. Petroleum ether (60–80 °C) was added into the resulting blue solution to precipitate a blue mass. This was dissolved in acetonitrile containing 2-aminothiophenol followed by addition of isopropanol and diethyl ether. The resulting solution upon keeping overnight at 4 °C yielded needle shaped dark blue diffraction quality crystals. Yield: 2.73 g (90%). *Anal.* Calc. for $MoC_{30}H_{45}N_7S_5$: C, 47.41; H, 5.96; N, 12.90; S, 21.09. Found: C, 47.38; H, 5.92; N, 12.86; S, 21.02%. Absorption spectrum (acetonitrile) λ_{max} (ϵ_M): 390 (10 120), 558 (8000) nm. IR (KBr pellet): v 2195 (CN), 3050 (aromatic CH stretching), 740 (aromatic CH bending) cm^{-1}.

*$[Et_4N]_2[W^{IV}(NH–(C_6H_4)–S)(mnt)_2]$ (**2a**):* To a solution of 2.96 g (4 mmol) of $[Et_4N]_2[W^{IV}O(mnt)_2]$ and 2.14 ml (20 mmol) of 2-aminothiophenol in 30 ml dichloromethane in cold was added 1 ml methanesulfonic acid dropwise with constant stirring. Petroleum ether (60–80 °C) was added into the resulting red solution to precipitate a red mass. This was dissolved in acetonitrile containing 2-aminothiophenol followed by addition of isopropanol and diethyl ether. The resulting solution upon keeping overnight at 4 °C yielded needle shaped red colored diffraction quality crystals. Yield: 3.04 g (90%). *Anal.* Calc. for $WC_{30}H_{45}N_7S_5$: C, 42.49; H, 5.35; N, 11.56; S, 18.91. Found: C, 42.44; H, 5.31; N, 11.52; S, 18.86%. Absorption spectrum (acetonitrile) λ_{max} (ϵ_M): 356 (12 960), 376 (13 060), 524 (4380) nm. IR (KBr pellet): v 2190 (CN), 3048 (aromatic CH stretching), 766 (aromatic CH bending) cm^{-1}.

*$[Ph_4P][Mo^{IV}(Et_2NS_2)(mnt)_2]$ (**1b**):* To a solution of 4.28 g (4 mmol) of $[Ph_4P]_2[Mo^{IV}O(mnt)_2]$ and 3.32 g (20 mmol) of $[NH_4][Et_2NS_2]$ in 30 ml dichloromethane in cold was added 1 ml methanesulfonic acid dropwise with constant stirring. Petroleum ether (60–80 °C) was added into the resulting purple solution to precipitate a purple mass. This was dissolved in acetonitrile followed by addition of isopropanol and diethyl ether. The resulting solution upon keeping overnight at 4 °C yielded block shaped deep purple diffraction quality crystals. Yield: 4.33 g (90%). *Anal.* Calc. for $MoC_{37}H_{30}N_5PS_6$: C, 51.44; H, 3.50; N, 8.10; S, 22.27. Found: C, 51.39; H, 3.46; N, 8.06; S, 22.22%. Absorption spectrum (acetonitrile) λ_{max} (ϵ_M): 365 (7540), 486 (7140), 530 (6420) nm. IR (KBr pellet): v 2190 (CN) cm^{-1}.

*$[PNP][W^{IV}(Et_2NS_2)(mnt)_2]$ (**2b**):* To a solution of 4.08 g (4 mmol) of $[PNP]_2[W^{IV}O(mnt)_2]$ and 3.32 g (20 mmol) of $[NH_4][Et_2NS_2]$ in 30 ml dichloromethane in cold was added 1 ml methanesulfonic acid dropwise with constant stirring. Petroleum ether (60–80 °C) was added into the resulting red solution to precipitate a red mass. This was dissolved in acetonitrile followed by addition of isopropanol and diethyl ether. The resulting solution upon keeping overnight at 4 °C yielded block shaped red diffraction quality crystals. Yield: 4.14 g (90%). *Anal.* Calc. for $WC_{49}H_{40}N_6P_2S_6$: C, 51.13; H, 3.50; N, 7.30; S, 16.71. Found: C, 51.09; H, 3.46; N, 7.26; S, 16.67%. Absorption spectrum (acetonitrile) λ_{max} (ϵ_M): 350 (6620), 415 (7180), 480 (5590) nm. IR (KBr pellet): v 2190 (CN) cm^{-1}.

2.3. X-ray crystallography

Suitable diffraction quality single crystals were obtained from the crystallization procedures described in each synthesis. The crystals used in the analyses were glued to glass fibers and mounted on BRUKER SMART APEX diffractometer. The instrument was equipped with CCD area detector and data were collected using graphite-monochromated Mo Kα radiation ($\lambda = 0.71069$ Å) at low temperature (100 K). Cell constants were obtained from the least-squares refinement of three-dimensional centroids through the use of CCD recording of narrow ω rotation frames, completing almost all-reciprocal space in the stated θ range. All data were collected with SMART 5.628 (BRUKER, 2003), and were integrated with the BRUKER SAINT [40] program. The structure was solved using SIR97 [41] and refined using SHELXL-97 [42]. Crystal structures were viewed using ORTEP [43] and DIAMOND 3.1e. The empirical absorption correction was applied using SADABS, as described by Blessing [44]. The space group of the compounds was determined based on the lack of systematic absence and intensity statistics. Full-matrix least squares/difference Fourier cycles were performed which located the remaining non-hydrogen atoms. All non-hydrogen atoms were refined with anisotropic displacement parameters. Complex **1a** possesses two anions in its asymmetric unit of which one shows trigonal prismatic and the other one shows distorted trigonal prismatic geometry. Complex **1b** possesses two anions in its asymmetric unit both exhibiting distorted trigonal prismatic geometry. In one anion, the ethyl groups of diethyldithiocarbamate ligand are in eclipsed conformation and in the other anion they are in gauche conformation. Complex **2a** contains one anion in its asymmetric unit and shows a distorted trigonal prismatic structure whereas **2b** contains two anions in its asymmetric unit, both exhibiting trigonal prismatic geometry. Due to these reasons additional symmetry could not have been assigned.

2.4. Computational details

All calculations were performed using the GAUSSIAN 03 (Revision B.04) package [45] on an IBM PC platform. Molecular orbitals were visualized using ‘Gauss View’ and geometry optimized molecular structures were shown with DIAMOND 3.1e. Gas phase geometry optimization and population analysis of the molecular orbitals were carried out at DFT level. The method used was Becke’s three-parameter hybrid-exchange functional [46], the non-local correlation provided by the Lee et al. expression [47], and Vosko, Wilk, and Nuair 1980 local correlation functional (III) (B3LYP) [46,47]. 6–31G*+ basis set [48] was used for C, N, and H atoms and 6–311G*+ basis set [49,50] was used for S atom. The LANL2DZ basis set [51] and LANL2 pseudopotentials of Hay and Wadt [52,53] were used for Mo and W atoms. The optimized minima were characterized by harmonic-vibration-frequency calculation with the same method and basis set in which the minimum has no imaginary frequency.

3. Results and discussion

3.1. Synthesis and reactivity

The reactions [17–23] of complex, $[M^{IV}O(mnt)_2]^{2-}$ (M = Mo/W) [17,39] under protic conditions suggest that the $\{M^{IV}{=}O\}$ moiety behaves like the carbonyl group. Thus $\{M{=}O\}$ bond can easily be protonated with the addition of an acid (HX) which may yield an intermediate species, $\{M^{IV}(OH)(X)\}$ (M = Mo/W) and when the counter anion, X is a non coordinating anion like methanesulfonate, the species responds to hydrolysis to yield the stable tris [5,25–34] species, $[M^{IV}(mnt)_3]^{2-}$ (M = Mo, **1c**; M = W, **2c**) in 67% yield (based on molybdenum/tungsten). Its formation can be near quantitative upon addition of one equivalent of free mnt [35–38] anion into the reaction medium [18]. Addition of 2-aminothiophenol and ammonium salt of N,N-diethyldithiocarbamate into this reaction medium yielded the complexes, $[Et_4N]_2[M^{IV}(NH–(C_6H_4)–S)(mnt)_2]$ (M = Mo, **1a**; M = W, **2a**), $[Ph_4P][Mo^{IV}(Et_2NS_2)(mnt)_2]$ (**1b**) and $[PNP][W^{IV}(Et_2NS_2)(mnt)_2]$ (**2b**) (Scheme 1). Absorption spectroscopic signatures of these complexes are shown in Fig. 1, which are dominated by ligand (2-aminothiophenolate/N,N-diethyldithiocarbamate) to metal charge transfer bands. Desoxo bis(dithiolene) complexes have earlier been shown by us to undergo axial ligand exchange reactions leading to interconversion of synthetic complexes [20,23]. It has also been shown that in solution these desoxo complexes slowly converted to the thermodynamically stable tris chelated complexes [20,23]. However, complexes **1a**, **2a** and **1b**, **2b** have been found to be unable to undergo interconversion among them (Scheme 1). Unlike the extreme stability of **1b** and **2b**, complexes **1a** and **2a** are unstable and decompose readily both in solid and in solution state and among them **2a** is more unstable than **1a**. This unusual instability of the mixed-ligand tris chelated complexes (**1a** and **2a**) may be a manifestation of hard-soft ligand donor effect. Nitrogen being a hard donor cannot stabilize the soft Mo(IV) like sulfur (a soft donor). Eventually complexes **1a** and **2a** can only be stabilized in solution in presence of excess 2-aminothiophenol. Degradation of **1a** and **2a** in solution are monitored by absorption spectroscopic measurements which are shown in Fig. 2. The intensity of the initial absorption band at 558 (**1a**) and 524 nm (**2a**) decrease with time and the spectroscopic nature of the final product indicates decomposition of the complexes involving ligand loss rather than the formation of tris(dithiolene) species or the starting material, $[M^{IV}O(mnt)_2]^{2-}$. Infact, complexes **1a** and **2a** cannot be converted to the corresponding tris (dithiolene) complexes **1c** and **2c**. Even in the presence of excess of mnt [35–38] anion into a solution of **1a** or **2a** such conversion did not occur. On the other hand, tris chelated complexes, **1c** and **2c** cannot be reverted back to either, **1a**, **2a** or to **1b**, **2b** (Scheme 1).

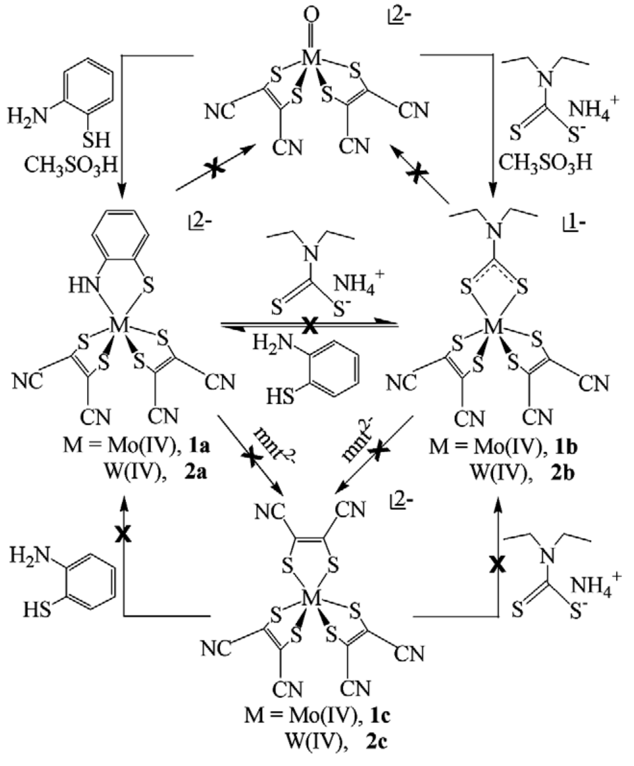

Scheme 1. Schematic diagram for the synthesis and no possible interconversion of the synthesized complexes.

3.2. X-ray structure description

All the four complexes (**1a**, **1b**, **2a** and **2b**) are characterized by X-ray structure determinations. Important structural parameters are summarized in Table 1 and important bond lengths are shown in Table 2. Structures (ORTEP view) of the four complexes are shown in Fig. 3. While trigonal prismatic co-ordination remains a distinct possibility in symmetric tris chelated complexes, it is somewhat more likely that mixed-ligand tris chelated complexes may adopt structures between octahedral and trigonal prismatic geometry. In order to complete the comparative study, we have synthesized and characterized complex **1b** by a new protonation method

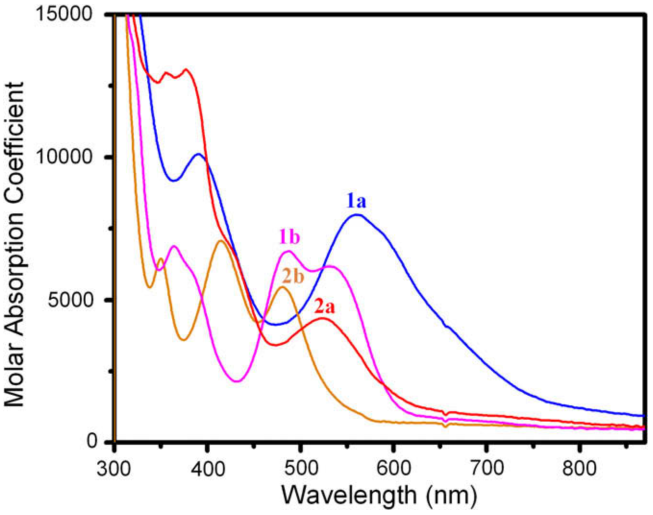

Fig. 1. Absorption spectroscopic signature of the complexes **1a**, **1b**, **2a** and **2b** in acetonitrile.

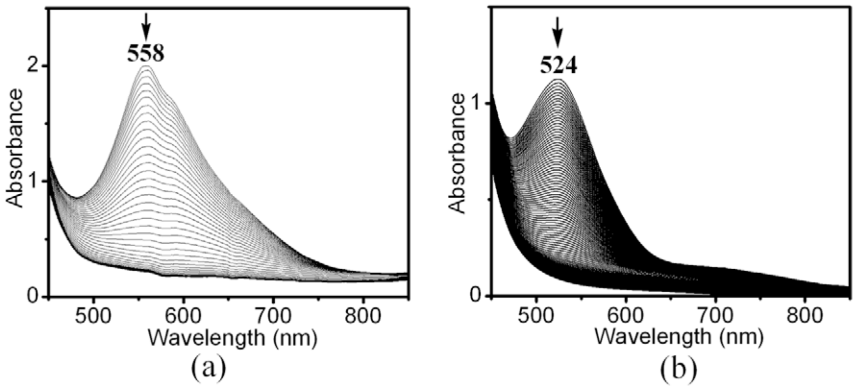

Fig. 2. Degradation of **1a** (a) and **2a** (b) in acetonitrile. Concentration of **1a** = 2×10^{-4} M, total time = 6 h, scan rate = 4 min/scan; concentration of **2a** = 2×10^{-4} M, total time = 10 min, scan rate = 4 s/scan.

Table 1
Crystallographic data[a] for complexes **1a**, **1b**, **2a** and **2b**.

Complexes	1a	1b	2a	2b
Formula	$C_{60}H_{90}Mo_2N_{14}S_{10}$	$C_{37}H_{30}MoN_5PS_6$	$C_{30}H_{45}WN_7S_5$	$C_{49}H_{40}WN_6P_2S_6$
Formula weight	1520.04	863.99	847.92	1151.07
Crystal system	triclinic	monoclinic	triclinic	triclinic
Space group	$P1$	$P2_1$	$P\bar{1}$	$P1$
T (K)	100	100	100	100
Z	1	4	2	2
a (Å)	7.215(5)	7.780(5)	10.214(5)	12.062(5)
b (Å)	13.772(5)	21.712(5)	13.065(5)	13.764(5)
c (Å)	18.063(5)	23.196(5)	14.085(5)	15.598(5)
α (°)	87.984(5)	90.000(5)	83.563(5)	79.611(5)
β (°)	84.861(5)	90.532(5)	72.306(5)	74.082(5)
γ (°)	83.872(5)	90.000(5)	81.564(5)	84.193(5)
V (Å^3)	1776.8(15)	3918(3)	1766.7(13)	2445.8(16)
D_{calc} (g/cm^3)	1.421	1.465	1.594	1.563
μ (mm^{-1})	0.695	0.729	3.597	2.725
θ range (°)	2.26–28.36	1.99–28.35	2.11–28.37	2.20–28.30
Goodness of fit (GOF) (F^2)	1.056	1.056	1.144	1.185
R_1[b] (wR_2[c])	0.0953 (0.1865)	0.0811 (0.1739)	0.0770 (0.1610)	0.0557 (0.1276)

[a] Mo Kα radiation.
[b] $R_1 = \sum||F_o| - |F_c||/\sum|F_o|$.
[c] $wR_2 = \{\sum[w(F_o^2 - F_c^2)^2]/\sum[w(F_o^2)^2]\}^{1/2}$.

Table 2
Important bond distances for complexes **1a**, **1b**, **2a** and **2b**.

Complexes	M–N$_{aminothiophenol}$ (Å)	M–S$_{aminothiophenol}$ (Å)	M–S$_{diethyldithiocarbmate}$ (Å)
$[Et_4N]_2[Mo^{IV}(NH–(C_6H_4)–S)(mnt)_2]$ (**1a**)	2.030	2.378	
$[Et_4N]_2[W^{IV}(NH–(C_6H_4)–S)(mnt)_2]$ (**2a**)	2.044	2.375	
$[Ph_4P][Mo^{IV}((Et_2NS_2)(mnt)_2]$ (**1b**)			2.435, 2.461
$[PNP][W^{IV}((Et_2NS_2)(mnt)_2]$ (**2b**)			2.478, 2.458

developed recently in dithiolene chemistry [20–23]. Its X-ray structure shows that complex **1b** adopts a distorted trigonal prismatic geometry in contrast to the trigonal prismatic geometry reported earlier [24]. Interestingly, complex **1a** possesses two anions in its asymmetric unit of which one shows trigonal prismatic and the other one shows distorted trigonal prismatic geometry. Complex **2a** contains one anion in its asymmetric unit and shows a distorted trigonal prismatic structure where as **2b** contains two anions in its asymmetric unit, both exhibiting almost trigonal prismatic geometry (deviation = 1.05°). Different structural geometry adapted by complexes **1a**, **2a**, **1b** and **2b** are shown in Supplementary material. Adaptation of either distorted trigonal prismatic or trigonal prismatic geometry by these mixed-ligand tris chelated complexes (**1b**, **2a**, **2b**) and the presence of both trigonal prismatic and distorted trigonal prismatic geometries in the crystal structure of complex **1a** strongly indicate that there may be equilibrium between these two structural entities in solution.

3.3. Electrochemistry

The electrochemical properties of these complexes are investigated by cyclic voltammetry and by differential pulse polarography (Figs. 4 and 5). Both **1a** and **2a** exhibited two sequential one electron oxidation steps (Fig. 4). Complex **1a** exhibited two sequential reversible oxidations at $E_{1/2} = 0.157$ V ($\Delta E_{pp} = 66$ mV, $I_{pa}/I_{pc} = 1.01$) and at $E_{1/2} = 0.660$ V ($\Delta E_{pp} = 76$ mV, $I_{pa}/I_{pc} = 1.06$). The first oxidation in such low potential is due to Mo^{IV}/Mo^{V} couple whereas the second one may be due to the oxidation of coordinated 2-aminothiophenolate ligand. In contrast, **2a** exhibited one reversible oxidation at $E_{1/2} = 0.034$ V ($\Delta E_{pp} = 52$ mV, $I_{pa}/I_{pc} = 1.12$) due to

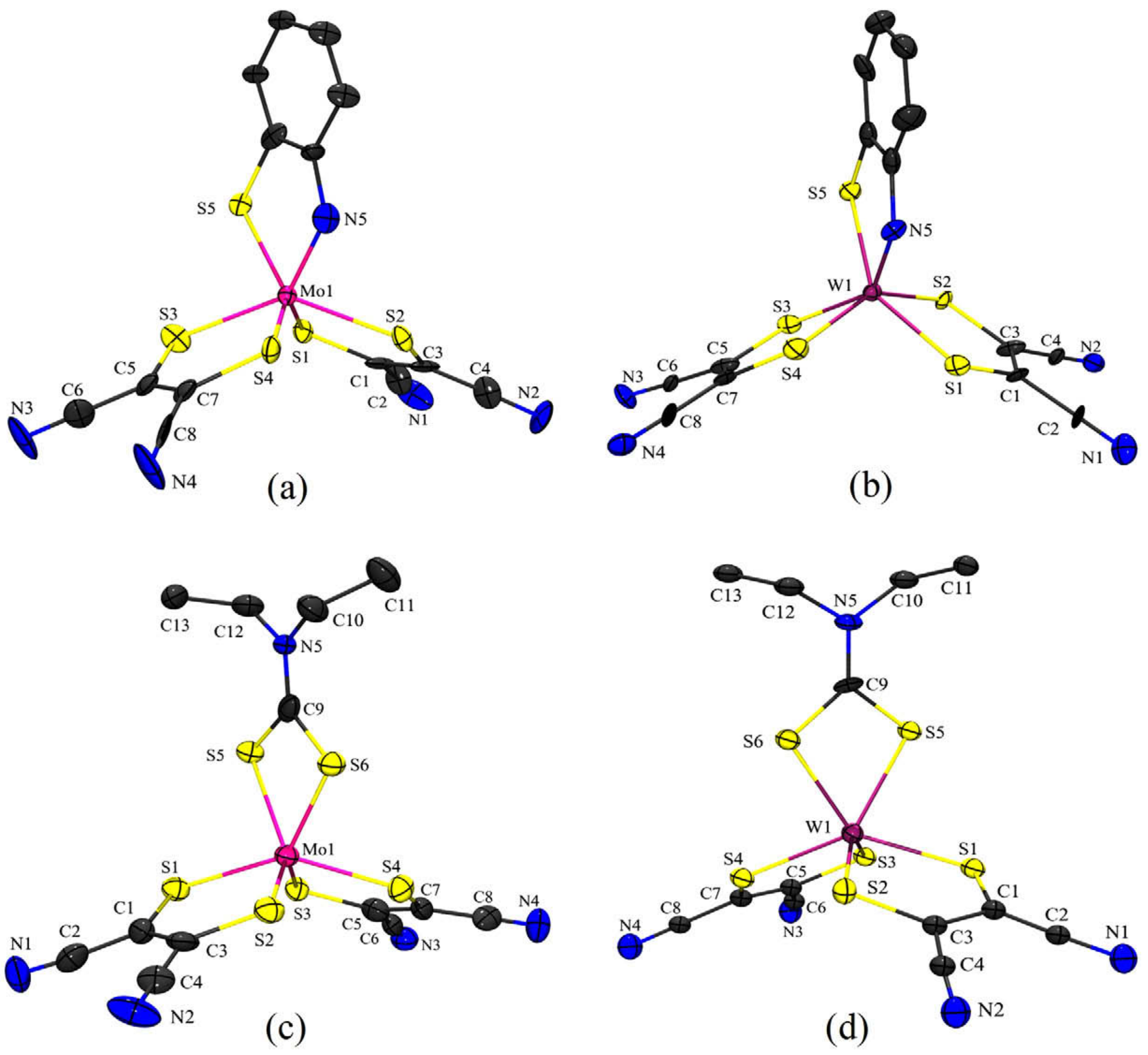

Fig. 3. Structure (ORTEP view) of anions of **1a** (a), **2a** (b), **1b** (c) and **2b** (d), showing 50% thermal probability ellipsoids with partial atom labeling scheme. Hydrogen atoms have been omitted for clarity.

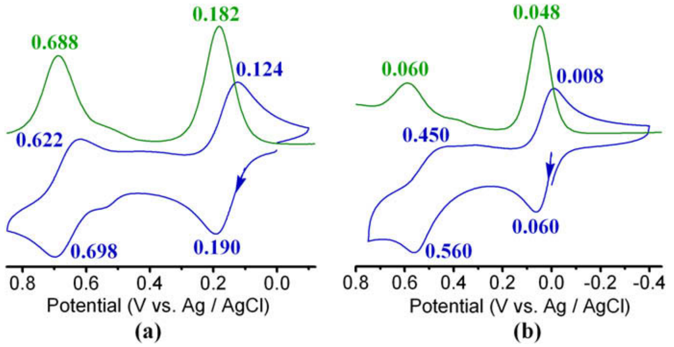

Fig. 4. Cyclic voltammograms (solid line) (scan rate = 100 mV/s) and differential pulse polarographs (dotted line) (scan rate = 20 mV/s, pulse width = 50 ms, pulse period = 200 ms, pulse amplitude = 50 mV) for the complexes **1a** (a) and **2a** (b) in acetonitrile.

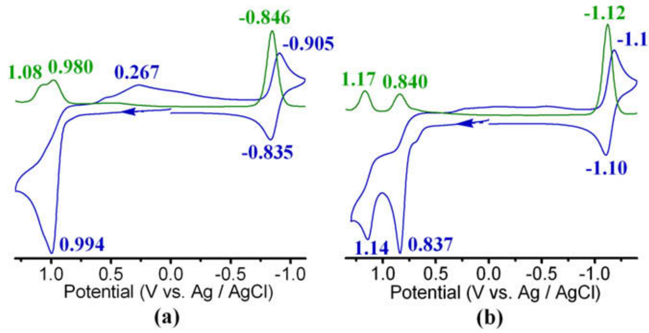

Fig. 5. Cyclic voltammograms (solid line) (scan rate = 100 mV/s) and differential pulse polarographs (dotted line) (scan rate = 20 mV/s, pulse width = 50 ms, pulse period = 200 ms, pulse amplitude = 50 mV) for the complexes **1b** (a) and **2b** (b) in acetonitrile.

W^{IV}/W^{V} followed by one irreversible oxidation at $E_{pa} = 0.560$ V due to coordinated 2-aminothiophenolate ligand. Complexes **1a** and **2a** did not show any reductive response up to −1.2 V (not shown in the figure). On the other hand, **1b** exhibited one reversible reduction at $E_{1/2} = -0.870$ V ($\Delta E_{pp} = 70$ mV, $I_{pa}/I_{pc} = 1.02$) and one irreversible oxidation at $E_{pa} = 0.994$ V (Fig. 5a). Complex **2b** exhibited one reversible reduction at $E_{1/2} = -1.14$ V ($\Delta E_{pp} = 80$ mV, $I_{pa}/I_{pc} = 0.91$) and two irreversible oxidations at $E_{pa} = 0.837$ V and

E_{pa} = 1.14 V (Fig. 5b). These two oxidations at E_{pa} = 0.837 V and E_{pa} = 1.14 V can be attributed to the oxidation of W^{IV} center in **2b** and the coordinated mnt ligand, respectively. In the case of **1b** these two oxidations (oxidation of Mo^{IV} center and oxidation of coordinated mnt ligand) are almost merged as indicated from corresponding differential pulse polarography presented in Fig. 5a.

3.4. EPR spectroscopic investigation

The reversible oxidations exhibited by **1a** and **2a** at such low potential (Fig. 4) prompted us to check the possibility of their one electron chemical oxidation. Complex **1a** was treated with sub equivalent (∼0.25 equivalent) amount of iodine in acetonitrile solution and the resultant solution was found to exhibit an EPR signal centered at g = 1.995 with well resolved $Mo^{95,97}$ hyperfine splitting (A/G = 36.2 ± 0.5) at room temperature (see Supplementary material). Complex **2a**, under similar treatment, showed an EPR signal centered at g = 1.975, although hyperfine splitting due to W is not well resolved (see Supplementary material). The resultant solutions although remained stable for few minutes at room temperature, but all attempts to isolate the oxidized species ended up with uncharacterized products.

3.5. Theoretical calculations and correlations with experimental results

The different electrochemical behavior of these closely related desoxo complexes can be rationalized in the light of relative energy levels of their molecular orbitals. At least in a qualitative sense a gas phase DFT calculation has been found to be successful to interpret the observed electrochemical data and their stability pattern. DFT calculations were carried out by employing a B3LYP hybrid functional using the GAUSSIAN 03 program [45] (see Section 2.4). Geometry of all the synthesized complexes were optimized (see Supplementary material) using the coordinates obtained initially from the X-ray crystallographic structure determination, followed

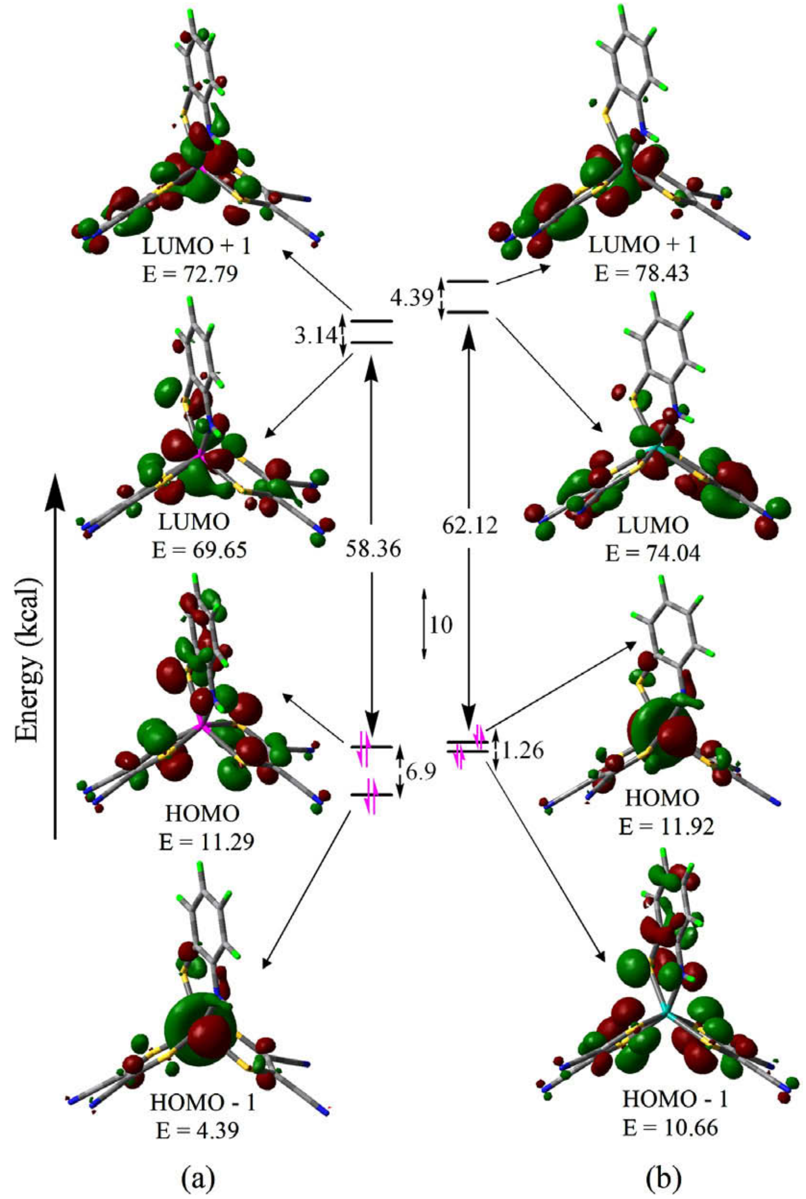

Fig. 6. Relative energy level diagram for the selected molecular orbitals of complex **1a** (a) and **2a** (b). Isosurface cut off value = 0.04. Color code for atoms: pink, molybdenum; sky blue, tungsten; yellow, sulfur; blue, nitrogen; grey, carbon; green, hydrogen. (For interpretation of the references to color in this figure legend, the reader is referred to the web version of this article.)

by single point energy calculation (Figs. 6–8). The assignment of the type of each MO was made on the basis of its composition and by visual inspection of its localized orbital. The coordinate frames for both the compounds were assigned by the visual inspection of the d_{z^2} and d_{xy} orbital.

From X-ray structure determination, **2a** has been found to adopt a distorted trigonal prismatic geometry whereas **1a** contains two anions in its asymmetric unit, of which one is trigonal prismatic and the other one is distorted trigonal prismatic in geometry. Upon geometry optimization both **1a** and **2a** adopted a distorted trigonal prismatic geometry. On the other hand, X-ray structure shows that **1b** adopts a distorted trigonal prismatic geometry and **2b** adopts a trigonal prismatic geometry, although upon geometry optimization, geometry in both the cases are found to be trigonal prismatic. Due to these reasons, single point calculation has also been performed with **1a** (using trigonal prismatic geometry as of **1a**) and with **1b** (using distorted trigonal prismatic geometry of **1b**) and the selected molecular orbitals are shown in Fig. 8.

Different stability pattern of the synthesized complexes can be rationalized with the aid of relative energy level diagrams of their selected molecular orbitals. These are shown in Figs. 6–8 and the metal contribution in the HOMOs and LUMOs of the complexes are summarized in Supplementary material. One interesting feature observed is that the HOMO and LUMO are essentially interchanged in the case of molybdenum and tungsten complexes with both 2-aminothiophenolato ligand (**1a** and **2a**, Fig. 6) and N,N-diethyldithiocarbamate ligand (**1b** and **2b**, Fig. 7). Fig. 6 shows that the HOMO in **1a** is predominantly ligand centered whereas in **2a**, it is predominantly metal centered (mainly metal d_{z^2}). Same situation prevails in case of **1b** and **2b**. Instability of the synthesized mixed-ligand tris chelated complexes, **1a** and **2a**, in comparison to the extreme stability of the symmetric tris chelated complexes of mnt (**1c** and **2c**) are in agreement with relatively higher energy HOMOs (Fig. 6) in case of **1a** (11.29 kcal) and **2a** (11.92 kcal) compared to relatively deeply buried HOMOs (see Supplementary material) in case of **1c** (−5.64 kcal) and **2c**

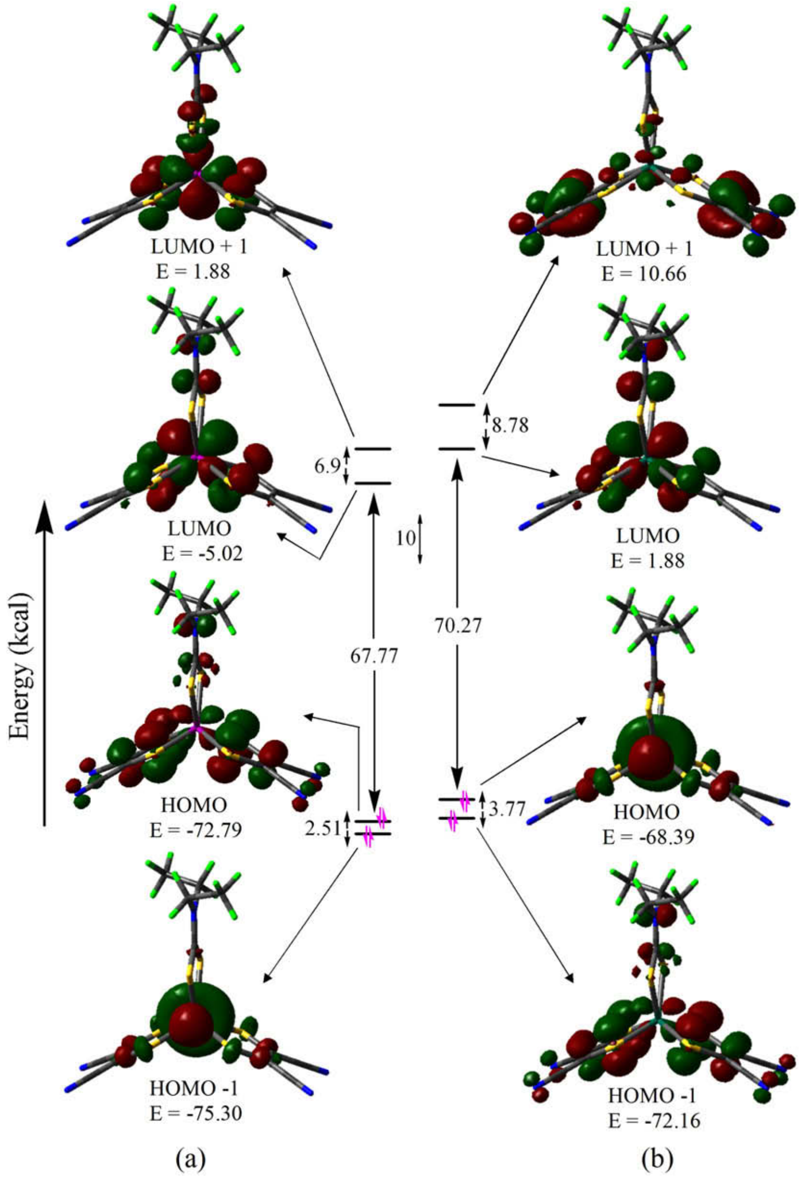

Fig. 7. Relative energy level diagram for the selected molecular orbitals of complex **1b** (a) and **2b** (b). Isosurface cut off value = 0.04. Color code for atoms: pink, molybdenum; sky blue, tungsten; yellow, sulfur; blue, nitrogen; grey, carbon; green, hydrogen. (For interpretation of the references to color in this figure legend, the reader is referred to the web version of this article.)

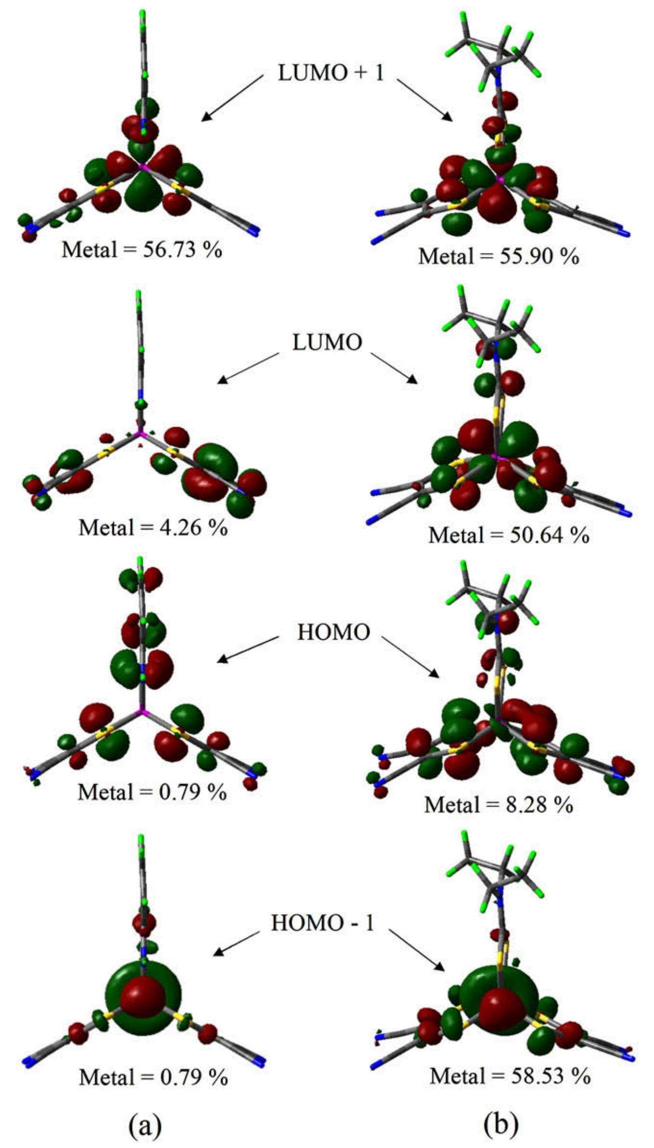

Fig. 8. Selected molecular orbitals of complexes **1a** ((a), geometry is trigonal prismatic) and **1b** ((b), geometry is distorted trigonal prismatic). Isosurface cut off value = 0.04. Color code for atoms: pink, molybdenum; yellow, sulfur; blue, nitrogen; grey, carbon; green, hydrogen. (For interpretation of the references to color in this figure legend, the reader is referred to the web version of this article.)

(−6.27 kcal). Eventually complexes **1a** and **2a** can only be stabilized in solution in presence of excess 2-aminothiophenol. Complexes **1b** and **2b** are highly stable in solution as well as in solid state and this are exhibited by their deeply buried HOMOs and LUMOs (Fig. 7). Infact, the relative energy level diagram indicates **1b** and **2b** to be more stable compared to even **1c** and **2c**.

Comparing Figs. 6a and 8a, it becomes evident that the nature of the LUMO changes upon using two different possible geometries of **1a**, namely, distorted trigonal prismatic (Fig. 6a, metal centered) and trigonal prismatic (Fig. 8a, ligand centered) although the character of molecular orbital remains almost same in the case of **1b** by using these two different possible geometries (Figs. 7a and 8b).

Electrochemical behavior of the synthesized complexes can be explained in the light of these relative energy level diagrams. LUMOs of both the complexes **1b** and **2b** are predominantly metal centered (mainly metal $d_{x^2-y^2}$). A reversible reduction at $E_{1/2} = -0.870$ V and $E_{1/2} = -1.14$ V in case of **1b** and **2b**, respectively, can be attributed to their low lying metal centered LUMOs (Fig. 7). A deeply buried HOMO ($E = -72.79$ kcal/mol) with large ligand contribution (Fig. 7) can well account for an irreversible oxidation at $E_{pa} = 0.994$ V in the case of **1b**. Irreversible oxidation at somewhat lower potential ($E_{pa} = 0.837$) in the case of **2b** is in agreement with its relatively less buried HOMO (Fig. 7) although a predominantly metal centered HOMO (mainly metal d_{z^2}) in this case, does not account for the irreversible character of the oxidation step. Rather it should support an expected reversible oxidation step. Sequential reversible oxidation steps in the case of complexes **1a** and **2a** cannot be directly rationalized in the light of their relative energy level diagram (Fig. 6). A monomeric system with predominantly ligand centered HOMO may not account for the observed two sequential reversible oxidation steps as seen in the case of **1a**. This can only be possible because of the presence of 2-aminothiophenolate ligand which may be responsible for the second oxidation step. However in the case of **2a**, the presence of a metal centered HOMO (mainly metal d_{z^2}) can account for the reversible oxidation at a much lower potential ($E_{1/2} = 0.034$ V) followed by an irreversible oxidation which may be correlated with the possible structural change that might have happened during the second oxidation centered at 2-aminothiophenolate ligand. The observed absence of any reduction steps up to −1.2 V is a manifestation of the predominantly ligand centered LUMOs (centered mainly in mnt) in the case of **2a** and any possible reduction would have destabilized the dithiolene bonding to tungsten center followed by dissociation of mnt ligand. In the case of **1a**, although the LUMO is metal centered (mainly metal $d_{x^2-y^2}$), but it is engaged with ligand orbitals along with significant ligand character as shown in Fig. 6a. Apart from this fact, Fig. 8a shows that the LUMO of **1a** comes out to be predominantly ligand centered (metal = 4.26%) when the trigonal prismatic geometry of **1a** is used for single point calculation involving population analysis. Presence of this significant ligand character in the LUMO of **1a** can account for the observed absence of any reduction steps up to −1.2 V.

4. Conclusions

Four hitherto unknown mixed-ligand tris chelate complexes of molybdenum(IV) and tungsten(IV) containing two maleonitriledithiolate and one 2-aminothiophenolate or N,N-diethyldithiocarbamate ligand are synthesized by a simple protonation method and analyzed in comparison with symmetric tris chelate complexes, $[M^{IV}(mnt)_3]^{2-}$ (M = Mo/W). Adaptation of either distorted trigonal prismatic or trigonal prismatic geometry by these mixed-ligand tris chelated complexes (**1b**, **2a**, **2b**) and the presence of both trigonal prismatic and distorted trigonal prismatic geometries in the crystal structure of complex **1a** strongly indicate the possibility of equilibrium between these two types of geometries in solution. In spite of structural similarity and expected chelate effect stability in all these complexes, 2-aminothiophenolate ligated complexes have been found to be extremely unstable in solution towards decomposition. Difference in electrochemical behavior in these seemingly similar synthesized complexes is correlated with population analysis of the respective redox molecular orbitals obtained from theoretical calculations at DFT level. Sequential reversible oxidation steps in 2-aminothiophenolato complexes have been further investigated by EPR spectroscopy with their one electron oxidized species, which may have importance in the context of Mo(V)/W(V) state generated during the catalytic cycle of oxidoreductase class of molybdenum and tungsten enzymes.

Acknowledgments

A.M. acknowledges research assistantship from DST, India, and S.S. thanks DST, India, for funding the project.

Appendix A. Supplementary data

CCDC 698199, 698200, 698201 and 698202 contains the supplementary crystallographic data for this paper. These data can be obtained free of charge from The Cambridge Crystallographic Data Centre via http://www.ccdc.cam.ac.uk/data_request/cif. Supplementary data associated with this article can be found, in the online version, at doi:10.1016/j.ica.2009.03.036.

References

[1] R. Eisenberg, J. Ibers, J. Am. Chem. Soc. 87 (1965) 3776.
[2] A. Smith, G. Schrauzer, V. Mayweg, J. Am. Chem. Soc. 87 (1965) 5798.
[3] R. Eisenberg, J. Ibers, Inorg. Chem. 15 (1966) 411.
[4] E.I. Stiefel, R. Eisenberg, R. Rosenberg, H.B. Gray, J. Am. Chem. Soc. 88 (1966) 2956.
[5] G. Brown, E.I. Stiefel, Inorg. Chem. 12 (1973) 2140.
[6] A. Cervilla, E. Llopis, D. Marco, F. Perez, Inorg. Chem. 40 (2001) 6525.
[7] S. Campbell, S. Harris, Inorg. Chem. 35 (1966) 3285.
[8] A.L. Tenderholt, R.K. Szllagyl, R.H. Holm, K.O. Hodgson, B. Hedman, E.I. Solomon, Inorg. Chem. 47 (2008) 6382.
[9] B.S. Lim, J.P. Donahue, R.H. Holm, Inorg. Chem. 39 (2000) 263.
[10] D.C. Olson, V.P. Mayweg, G.N. Schrauzer, J. Am. Chem. Soc. 88 (1966) 4876.
[11] E.I. Stiefel, W.E. Newton, N. Pariyadath, in: P.C.H. Mitchell (Ed.), Proceedings of the Climax International Conference on the Chemistry and Uses of Molybdenum, Climax Molybdenum Co., 1977, p. 265.
[12] E.I. Stiefel, in: P.C.H. Mitchell (Ed.), Proceedings of the Climax First International Conference on the Chemistry and Uses of Molybdenum, Climax Molybdenum Co., 1974, p. 284.
[13] A. Butcher, P.C.H. Mitchell, in: P.C.H. Mitchell (Ed.), Proceedings of the Climax First International Conference on the Chemistry and Uses of Molybdenum, Climax Molybdenum Co., 1974, p. 285.
[14] L.N. Duglav, Z.I. Usmanov, Zhur. Strukt. Khim. 16 (1975) 312.
[15] I.N. Marov, V.K. Belyaeva, A.N. Ermakov, Y.N. Dubrov, Russ. J. Inorg. Chem. 14 (1969) 1391.
[16] N.S. Garifyanov, S.E. Kamenev, I.V. Ovchinnikov, Russ. J. Phys. Chem. 43 (1969) 5.
[17] S.K. Das, P.K. Chaudhury, D. Biswas, S. Sarkar, J. Am. Chem. Soc. 116 (1994) 9061.
[18] S.K. Das, D. Biswas, R. Maiti, S. Sarkar, J. Am. Chem. Soc. 118 (1996) 1387.
[19] K. Nagarajan, H.K. Joshi, P.K. Chaudhury, K. Pal, J.J.A. Cooney, J.H. Enemark, S. Sarkar, Inorg. Chem. 43 (2004) 4532.
[20] A. Majumdar, K. Pal, K. Nagarajan, S. Sarkar, Inorg. Chem. 46 (2007) 6136.
[21] A. Majumdar, J. Mitra, K. Pal, S. Sarkar, Inorg.Chem. 47 (2008) 5360.
[22] A. Majumdar, K. Pal, S. Sarkar, J. Am. Chem. Soc. 128 (2006) 4196.
[23] A. Majumdar, K. Pal, S. Sarkar, Inorg. Chem. 47 (2008) 3393.
[24] W.P. Bosman, A. Nieuwpoort, Inorg. Chem. 15 (1976) 775.
[25] H.-W. Xu, Z.-N. Chen, J.-G. Wu, Acta Crystallogr., Sect. E: Struct. Rep. Online 58 (2002) m631.
[26] D.V. Formitchev, B.S. Lim, R.H. Holm, Inorg. Chem. 40 (2001) 645.
[27] K. Wang, J.M. McConnachie, E.I. Stiefel, Inorg. Chem. 38 (1999) 4334.
[28] G. Matsubayashi, K. Douki, H. Tamura, M. Nakano, W. Mori, Inorg. Chem. 32 (1993) 5990.
[29] M. Draganjac, D. Coucouvanis, J. Am. Chem. Soc. 105 (1983) 139.
[30] E. Smith, G.N. Schrauzer, V.P. Mayweg, W. Heinrich, J. Am. Chem. Soc. 87 (1965) 5798.
[31] M. Cowie, M.J. Bennett, Inorg. Chem. 15 (1976) 1584.
[32] S. Boyde, C.D. Garner, J.H. Enemark, R.B. Ortega, J. Chem. Soc., Dalton Trans. (1987) 2267.
[33] C.A. Goddard, R.H. Holm, Inorg. Chem. 38 (1999) 5389.
[34] X. Yang, G.K.W. Freeman, T.B. Rauchfuss, S.R. Wilson, Inorg. Chem. 30 (1991) 3034.
[35] G. Bahr, B. Schleltzer, Chem. Ber. 88 (1955) 1771.
[36] G. Bahr, Angew. Chem. 68 (1956) 525.
[37] E.I. Stiefel, L.E. Bennet, Z. Dori, T.H. Crawford, C. Simo, H.B. Gray, Inorg. Chem. 9 (1970) 281.
[38] A. Davidson, R.H. Holm, Inorg. Synth. 10 (1967) 8.
[39] R. Maiti, K. Nagarajan, S. Sarkar, J. Mol. Struct. 656 (2003) 169.
[40] SAINT, Version 5.6, Bruker AXS Inc., Madison, WI, 2000.
[41] A. Altomare, M.C. Burla, M. Camalli, G.L. Cascarano, C. Giacovazzo, A. Guagliardi, A.G.G. Moliterni, G. Polidori, R. Spagna, J. Appl. Crystallogr. 32 (1999) 115.
[42] G.M. Sheldrick, SHELX97, Programs for Crystal Structure Analysis (Release 97-2), University of Göttingen, Germany, 1997.
[43] L.J. Farrugia, J. Appl. Crystallogr. 30 (1997) 565.
[44] R.H. Blessing, Acta Crystallogr. A51 (1995) 33.
[45] M.J. Frisch, G.W. Trucks, H.B. Schlegel, G.E. Scuseria, M.A. Robb, J.R. Cheeseman, J.A. Montgomery Jr., T. Vreven, K.N. Kudin, J.C. Burant, J.M. Millam, S.S. Iyengar, J. Tomasi, V. Barone, B. Mennucci, M. Cossi, G. Scalmani, N. Rega, G.A. Petersson, H. Nakatsuji, M. Hada, M. Ehara, K. Toyota, R. Fukuda, J. Hasegawa, M. Ishida, T. Nakajima, Y. Honda, O. Kitao, H. Nakai, M. Klene, X. Li, J.E. Knox, H.P. Hratchian, J.B. Cross, V. Bakken, C. Adamo, J. Jaramillo, R. Gomperts, R.E. Stratmann, O. Yazyev, A.J. Austin, R. Cammi, C. Pomelli, J.W. Ochterski, P.Y. Ayala, K. Morokuma, G.A. Voth, P. Salvador, J.J. Dannenberg, V.G. Zakrzewski, S. Dapprich, A.D. Daniels, M.C. Strain, O. Farkas, D.K. Malick, A.D. Rabuck, K. Raghavachari, J.B. Foresman, J.V. Ortiz, Q. Cui, A.G. Baboul, S. Clifford, J. Cioslowski, B.B. Stefanov, G. Liu, A. Liashenko, P. Piskorz, I. Komaromi, R.L. Martin, D.J. Fox, T. Keith, M.A. Al-Laham, C.Y. Peng, A. Nanayakkara, M. Challacombe, P.M.W. Gill, B. Johnson, W. Chen, M.W. Wong, C. Gonzalez, J.A. Pople, GAUSSIAN 03, Revision B.04, Gaussian Inc., Pittsburgh, PA, 2003.
[46] A.D. Becke, J. Chem. Phys. 98 (1993) 5648.
[47] C. Lee, W. Yang, R.G. Parr, Phys. Rev. B 37 (1988) 785.
[48] G.A. Patersson, M.A. Al-Laham, J. Chem. Phys. 94 (1991) 6081.
[49] A.D. McLean, G.S. Chandler, J. Chem. Phys. 72 (1980) 5639.
[50] R. Krishnan, J.S. Binkley, R. Seeger, J.A. Pople, J. Chem. Phys. 72 (1980) 650.
[51] P.J. Hay, W.R. Wadt, J. Chem. Phys. 82 (1985) 299.
[52] P.J. Hay, W.R. Wadt, J. Chem. Phys. 82 (1985) 270.
[53] W.R. Wadt, P.J. Hay, J. Chem. Phys. 82 (1985) 284.